

Isolated ionospheric disturbances as deduced from global GPS network

E. L. Afraimovich, E. I. Astafieva,
Institute of Solar-Terrestrial Physics SD RAS,
p. o. box 4026, Irkutsk, 664033, Russia,
fax: +7 3952 462557; e-mail: afra@iszf.irk.ru

Abstract

We investigate an unusual class of medium-scale traveling ionospheric disturbances (MS TIDs) of the nonwave type, isolated ionospheric disturbances (IIDs) that manifest themselves in total electron content (TEC) variations in the form of single aperiodic negative TEC disturbances of a duration of about 10 min (the total electron content spikes, TECS). For the first time, we present the TECS morphology for 170 days with a different level of geomagnetic activity and with the number of stations of the global GPS network ranging from 4 to 240. A total number of the TEC series (radio paths) used in the analysis, corresponding to the observation along a single receiver-satellite Line-of-Sight (LOS), with a duration of each series of about 2.3 hours, exceeded 850000. The data were obtained using the technology of global detection and monitoring of ionospheric disturbances (GLOBDET, developed at the ISTP SB RAS) of a natural and technogenic origin using measurements of TEC variations from a global network of receivers of the GPS. It was found that TECS are observed in no more than 1-2% of the total number of radio paths. We present the results derived from analyzing the dependence of TECS parameters on the local time, and on the level of geomagnetic activity. The TECS amplitude exceeds at least one order of magnitude the TEC fluctuation intensity under "background" conditions. The IID-induced TEC variations are similar in their amplitude, form and duration to the TEC response to shock-acoustic waves (SAW) generated during rocket launchings and earthquakes. However, the IID propagation velocity is less than

the SAW velocity (800-1000 m/s) and are most likely to correspond to the velocity of background medium-scale acoustic-gravity waves (AGW), on the order of 100-200 m/s.

Keywords

Ionosphere (ionospheric irregularities, instruments and techniques), radio science (ionospheric propagation)

1 Introduction

Of the known ionospheric irregularities of a different class, mid-latitude isolated ionospheric disturbances (IIDs) stand out as a highly unusual type. The past 40 years saw a consistent interest in the study of the origin of IIDs that was aroused due to difficulties in determining an adequate mechanism for IID generation in mid-latitudes, as well as by the fact that the IID have a marked effect on amplitude and phase characteristics of transionospheric signals from radio engineering communication and navigation systems (Afraimovich et al., 1992) by causing serious malfunctions of these systems.

A large number of publications (e.g., Karasawa, 1985; Titheridge, 1971), including a review by Bowman (1989) were devoted to the study along this line. IIDs are detected when recording amplitude and phase scintillations of transionospheric radio signals in the form of rarely occurring single aperiodic negative impulses with a duration from a few to several tens of seconds (Karasawa, 1985). To name this uncommon type of scintillation Karasawa (1985) seems to be the first to coin the term "spikes-type" (S-) scintillations.

Karasawa et al. (1985) noticed from a long-term recording of the signal from the geostationary MARISAT satellite at 1.5 GHz frequency that synchronous with amplitude S-scintillations, there occur similar-appearing changes of the rotation angle of polarization plane that are proportional to a corresponding disturbance of total electron content (TEC). Anomalous fluctuations, recorded during 13 months of observation, occur predominantly in the night-time and last from 5 s to 2 min. The diurnal dependence of the S-type oscillations shows two distinct peaks: 09:00-15:00 in the daytime, and 20:00-01:00 at night. As far as the seasonal dependence is concerned, however, a maximum of the oscillation distribution corresponds to early summer (June). It is cus-

tomary to associate the occurrence of S-type oscillations with diffraction or interference from small-scale irregularities, "blobs" and "bubbles", generated in the ionosphere.

Titheridge (1971) found that amplitude and phase S-scintillations are caused by refraction and diffraction effects at the propagation of the transionospheric signal in a medium with IIDs and presented the corresponding formulae for estimating these effects as a function of relationship of the wavelength of the radio wave, the irregularity size and the sounding geometry (LOS to the satellite and the distance to the layer with IIDs).

However, in spite of the many years of experimental and theoretical investigations, there is as yet no clear understanding not only of the physical nature of IIDs but even of their morphology (the occurrence frequency as a function of geographical position, time, level of geomagnetic and meteorological activity, etc.).

To tackle these questions requires statistically significant sets of experimental data with good spatial and temporal resolution in order to gain insight into not only morphological but also dynamic IID characteristics: the direction of travel, the propagation velocity, and the location of the possible disturbance source. Another important requirement implies a continuity and global coverage of observations since such phenomena are relatively rare in time and random in space.

Such an opportunity is for the first time provided by the use of the international ground-based network of two-frequency receivers of the GPS, consisting of no less than 1000 sites as of the beginning of 2002 and posting its data on the Internet, which open up new avenues for a global, continuous, fully computerized monitoring of ionospheric disturbances of a different class. Analysis and detection of IIDs was made possible through the use of the technology for global detection and determination of parameters of ionospheric disturbances of a different class that was developed at the ISTP (Afraimovich, 2000b).

The objective of this paper is to study the morphology and spatial and temporal properties of IIDs using data from a global network of GPS receivers. Following Karasawa et al. (1985), the term TECS (total electron content spikes) will be used here to designate the IID-induced TEC disturbances. The sample statistic of the occurrence frequency and morphology used in this study does refer to TECS recorded from GPS data. Within the framework of certain model representations, using these data it is possible to reconstruct amplitude and spatial characteristics of local electron density

disturbances, i.e. of IIDs themselves. On this basis, the term IIDs will be used below interchangeably with the term TECS.

Section 2 describes the method for detecting the TECS obtained in our study. Section 3 presents the TECS morphology. Section 4 is devoted to a detailed analysis of the spatial and temporal properties of IIDs by considering the most pronounced manifestation of TECS on October 5, 2001 in California, USA. The discussion of results compared with findings reported by other authors is presented in Section 5.

Our comparison of IID characteristics with geomagnetic field variations used data from near-lying magnetic variation stations of the INTERMAGNET network (address: <http://www.intermagnet.org>).

2 Method of processing the data from the global network. Selection of TECS

The standart GPS technology provides a means for wave disturbances detecion based on phase measurements of TEC at each of spaced two-frequency GPS receivers (Hofmann-Wellenhof et. al, 1992):

$$I_o = \frac{1}{40.308} \frac{f_1^2 f_2^2}{f_1^2 - f_2^2} [(L_1 \lambda_1 - L_2 \lambda_2) + const + nL], \quad (1)$$

where $L_1 \lambda_1$ and $L_2 \lambda_2$ are additional paths of the radio signal caused by the phase delay in the ionosphere, (m); L_1 and L_2 represent the number of phase rotations at the frequencies f_1 and f_2 ; λ_1 and λ_2 stand for the corresponding wavelengths, (m); *const* is the unknown initial phase ambiguity, (m); and nL are errors in determining the phase path, (m).

Phase measurements in the GPS can be made with a high degree of accuracy corresponding to the error of TEC determination of at least 10^{14} m^{-2} when averaged on a 30-second time interval, with some uncertainty of the initial value of TEC, however (Hofmann-Wellenhof et. al, 1992). This makes possible detecting ionization irregularities and wave processes in the ionosphere over a wide range of amplitudes (up to 10^{-4} of the diurnal TEC variation) and periods (from 24 hours to 5 min). The unit of TEC *TECU*, which is equal to 10^{16} m^{-2} and is commonly accepted in the literature, will be used in the following.

Primary data include series of "oblique" values of TEC $I_0(t)$, as well as the corresponding series of elevations $\theta_s(t)$ and azimuths $\alpha_s(t)$ of the LOS to the satellite calculated using our developed CONVTEC program which converts the GPS system standard RINEX-files on the INTERNET (Gurtner, 1993).

Series of the values of elevations $\theta_s(t)$ and azimuths $\alpha_s(t)$ of the LOS to the satellite were used to determine the coordinates of subionospheric points, and to convert the "oblique" TEC $I_0(t)$ to the corresponding value of the "vertical" TEC by employing the technique reported by Klobuchar (1986)

$$I = I_0 \times \cos \left[\arcsin \left(\frac{R_z}{R_z + h_{max}} \cos \theta_s \right) \right], \quad (2)$$

where R_z is the Earth's radius, and $h_{max}=300$ km is the height of the F_2 -layer maximum. All results in this study were obtained for elevations $\theta_s(t)$ larger than 30° .

The technology of global detection of TEC disturbances that was developed at the ISTEP SB RAS makes it possible to select - in the automatic mode from an extensive amount of experimental material - TEC disturbances which can be classed as TECS. TECS were selected by two criteria. TEC variations were selected first, the standard deviation (rms) of which exceeded the prescribed level ϵ . The statistic of TECS discussed in this paper was obtained for $\epsilon = 0.1$ *TECU*. Then, for each filtered series we verified the fulfilment of the "singleness" condition of the TEC overshoot.

Fig. 1 illustrates the TECS selection procedure. Fig. 1a presents an example of weakly disturbed disturbances of a "vertical" TEC $I(t)$ recorded on February 11, 2001 at station COCO (96.8°E ; 12.1°S ; the satellite number is PRN30). Fig. 1b presents the filtered (from the initial $I(t)$ -series) $dI(t)$ -variations. Thin horizontal lines show the prescribed threshold ϵ . The standard deviation of the $dI(t)$ -variations is 0.007 *TECU*, that is, does not reach the prescribed threshold, $\epsilon = 0.1$ *TECU*.

Figs. 1d and 1e plot the same dependencies as in Figs. 1a and 1b, but for station BAKO (106.8°E ; 06.5°S ; the satellite number is PRN26). It is evident from Fig. 1d that unusual (for background disturbances) TEC variations in the form of a single impulse of a duration on the order of $\Delta T=10$ min are clearly identified at the background of slow TEC variations.

The time t_{min} , corresponding to the value of A_{min} of the filtered TEC variation $dI(t)$, is shown in Fig.1e by the shaded triangle. The value of ΔT is determined from the level of $0.5 A_{min}$. The amplitude of this pulse A_{min} far exceeds the specified threshold

ϵ and at least an order of magnitude higher than the background TEC fluctuation intensity for this range of periods (Afraimovich et al., 2001b).

The relative amplitude of such a response A_{min}/I_0 has a significant value, 2%. We used, as the background value of I_0 , the absolute "vertical" TEC value $I_0(t)$ for the site located at 7.5°S; 105°E, obtained from IONEX-maps of TEC (Mannucci, 1998).

It should be noted that the above examples both refer to the same time interval and to the stations spaced by a distance over 1300 km. This indicates a local character of the phenomenon and is in agreement with the overall statistic characterizing its spatial correlation (see Section 3).

For each of the events satisfying the above TECS selection criteria, a special file was used to store information about the GPS station name and geographic latitude and longitude; GPS satellite PRN number; amplitude A_{min} ; time t_{min} corresponding to the minimum value of the A_{min} amplitude; and about the TECS duration ΔT . The sample statistic, presented below, was obtained by processing such files.

3 Morphology of TECS

A total number of the TEC series (radio paths) used in the analysis, corresponding to the observation along a single receiver-satellite LOS, with a duration of each series of about 2.3 hours, exceeded 850000. The method outlined above was used to obtain a set of TECS totaling about 10000 cases, or making up about 1% of the total number of the LOS's. An analysis of the resulting statistic revealed a number of dependencies of TECS parameters on different factors.

First we consider the seasonal dependence of the TECS occurrence frequency and amplitude (Fig. 2). Fig. 2a plots the number of days of observation M versus season. As is evident, the autumn is represented best statistically. Fig.2b shows the seasonal dependence of the number of TECS, N . Fig. 2c plots the number of TECS per day as a function of season $L = N/M$. This dependence has maxima in spring and in autumn.

The relative density of TECS, D , obtained as the ratio of the number of TECS identified, N , to the number of LOS's, is presented in Fig. 2d.

Vertical lines in Fig. 2d show TECS standard deviations (rms). The dashed horizontal line plots the threshold in amplitude $\epsilon = 0.1 \text{ TECU}$. The most probable value of $\langle |A_{min}| \rangle$ with a small scatter varies around the value 0.3 TECU , independently

of the season.

Fig. 3a plots the dependence $P(|Dst|)$ of the number of TECS on the modulus of values of the geomagnetic activity index Dst . There is a general tendency of the number of TECS to increase with the decreasing level of geomagnetic activity. Most (80%) of TECS occur when values of the Dst -index are below 50 nT.

Fig. 3b presents the diurnal distribution of TECS, $P(t_{min})$, for the times t_{min} corresponding to the minimum value of the amplitude A_{min} . It is evident that the distribution has maxima in the night-time and in the morning hours, approximately from 00:00 to 07:00, and from 23:00 to 24:00 of local time LT.

Fig. 3d presents the normalized probability distribution $P(|A_{min}|)$ of TECS occurrence with a given amplitude A_{min} . The vertical dashed line shows the threshold in amplitude $\epsilon = 0.1 \text{ TECU}$. It was found that the largest probable value of the amplitude $|A_{min}|$, also shown in Fig.3d, is about 0.3 TECU , and the half-width of the distribution is 0.2 TECU . As demonstrated by Afraimovich et al. (2001a), the mean values of the TEC variation amplitude with a period of 20 min for the magnetically quiet and magnetically disturbed days do not exceed 0.01 TECU and 0.07 TECU , respectively. Thus the most probable value of the amplitude A_{min} of the TECS identified here exceeds the mean values of the TEC phase variation amplitude by a factor of 4-5 as a minimum.

The availability of a large number of stations in some regions on the globe, for instance, in California, USA, and West Europe, furnishes an opportunity to determine not only the temporal but also spatial characteristics of TECS. In order to estimate the radius of spatial correlation of events of this type, the number of cases was calculated where TECS within a single 2.3-hour time interval were observed at any two GPS stations spaced by a distance dR . Fig. 3c presents the histogram of the number of such cases $P(dR)$ as a function of distance dR . It was found that the localization of TECS in space is sharply defined. In 90% of cases the distance dR does not exceed 500 km.

4 Dynamics and anisotropy of IIDs as deduced from the October 5, 2001 event over California, USA

The event of October 5, 2001 was used in the analysis of the TECS dynamic characteristics of TECS. On that day between 08:00 and 18:00 UT, a number of GPS stations located in California, USA (220-260°E; 28-42°N) recorded a large number of traveling ionospheric disturbances (TIDs) of the TECS type. For the above-mentioned time interval and the selected longitude range, the local time varied from 00:00 to 10:00 LT (for the longitude of 240°E corresponding to the center of the GPS station array used in the analysis). So that the experimental conditions were characteristic for the night-time ionosphere.

Fig. 4 illustrates the geometry of the experiment on October 5, 2001. Heavy dots show the GPS stations, and small dots indicate the position of subionospheric points for all LOS's. Since several (at least four) GPS satellites are observed at each receiving site simultaneously, the number of LOS's far exceeds the number of stations, which enhances considerably the possibilities of the analysis. Panel **a** presents the entire set of GPS stations and subionospheric points that were used in the experiment for the time interval from 8:00 to 10:00 UT. Panels **b** and **c** show the stations and subionospheric points where the TEC variations revealed TECS with an amplitude exceeding the specified threshold $\epsilon=0.01$ *TECU* (**b**), and $\epsilon=0.1$ *TECU* (**c**). Except in a single case, TECS were recorded along the LOS running over land. As is evident from the figure, the increase of the recording threshold did not change the number of events recorded.

Fig. 5 presents the geomagnetic field *Dst*-variations (**a**) for October 5, 2001. *H(t)*-variations of the horizontal component of the geomagnetic field as recorded at station Victoria (48.52°N; 236.58°E) - **b**. *dH(t)*-variations of the horizontal component of the geomagnetic field, filtered from the *H(t)*-series in the range of 2-20-min periods - **c**. At the lower time scale in Fig. 5, the local time LT is represented for the longitude of 240°E.

Fig. 5**d** presents the distribution of the values of the GPS station latitudes and time t_{min} , corresponding to each of the TECS detected that day by all GPS stations of the California region that were used in the analysis (220-260°E; 28-42°E). The letters

A, B, C, and D in Fig. 5d label the TECS "traces" that are presented in Fig. 6 on a smaller time scale (see Section 4.2). Fig. 5e - same as in Fig. 5d, but for the station longitudes and t_{min} .

Fig. 5f presents the distribution $N(t)$ of the number of TECS that were detected that day at all GPS stations used in the analysis, with the rms above $\epsilon=0.1$ *TECU*.

4.1 Determining the dynamic characteristics of IIDs by the SADM-GPS method

The methods of determining the form and dynamic characteristics of TIDs that are used in this study are based on those reported in (Mercier, 1986; Afraimovich, 1997; Afraimovich et al., 1998; 1999; 2000c).

We determine the velocity and direction of motion of the phase interference pattern (phase front) in terms of some model of this pattern, an adequate choice of which is of critical importance. In the simplest form, space-time variations in phase of the transionospheric radio signal that are proportional to TEC variations $dI(t, x, y)$ in the ionosphere, at each given time t can be represented in terms of the phase interference pattern that moves without a change in its shape (the non dispersive disturbances):

$$I(t, x, y) = F(t - x/u_x - y/u_y) \quad (3)$$

where $u_x(t)$ and $u_y(t)$ are the displacement velocities of intersection of the phase front of the axes x (directed to the East) and y (directed to the North), respectively.

It should be noticed, however, that in real situations this ideal model (3) is not realized in a pure form. This is because that the TIDs propagate in the atmosphere in the form of a dispersing wave packet with a finite value of the width of the angular spectrum. But in the first approximation on short time interval of averaging compared to time period of filtered variations of TEC, the phase interference pattern moves without a substantial change in its shape.

A Statistical, Angle-of-arrival and Doppler Method (SADM) was proposed by Afraimovich (1997) for determining the characteristics of the dynamics of the phase interference pattern in the horizontal plane by measuring variations of phase derivatives with respect to the spatial coordinates $I'_x(t)$, $I'_y(t)$, and to the time $I'_t(t)$. This permits the determination of the unambiguous orientation of $\alpha(t)$ of the wave-vector \mathbf{K} in the range 0...360° and the horizontal velocity $V(t)$ at each specific instant of time.

Afraimovich et al. (1998, 1999, 2000c) described updating of the SADM algorithm for GPS-arrays (SADM-GPS) based on a simple model for the displacement of the phase interference pattern that travels without a change in the shape and on using current information about the angular coordinates of the LOS: the elevation $\theta_s(t)$ and the azimuth $\alpha_s(t)$.

The method SADM-GPS makes it possible to determine the horizontal velocity $V_h(t)$ and the azimuth $\alpha(t)$ of TID displacement at each specific instant of time (the wave-vector orientation \mathbf{K}) in a fixed coordinate system (x, y) :

$$\begin{aligned}
\alpha(t) &= \arctan(u_y(t)/u_x(t)) \\
u_x(t) &= I'_t(t)/I'_x(t) = u(t)/\cos \alpha(t) \\
u_y(t) &= I'_t(t)/I'_y(t) = u(t)/\sin \alpha(t) \\
u(t) &= |u_x(t)u_y(t)|/(u_x^2(t) + u_y^2(t))^{-1/2} \\
V_x(t) &= u(t) \sin \alpha(t) + w_x(t) \\
V_y(t) &= u(t) \cos \alpha(t) + w_y(t) \\
V_h(t) &= (V_x^2(t) + V_y^2(t))^{1/2}
\end{aligned} \tag{4}$$

where w_x and w_y are the x and y projections of the velocity w of the subionospheric point (for taking into account the motion of the GPS satellite).

Let us take a brief look at the sequence of data handling procedures. Out of a large number of GPS stations, three points (A, B, C) are chosen in such a way that the distances between them do not exceed about one-half the expected wavelength Λ of the disturbance. The point B is taken to be the center of a topocentric frame of reference. Such a configuration of the GPS receivers represents a GPS-array (or a GPS-interferometer) with a minimum of the necessary number of elements. In regions with a dense network of GPS-points, we can obtain a broad range of GPS-arrays of a different configuration, which furnishing a means of testing the data obtained for reliability; in this paper we have taken advantage of this possibility (Section 4.2).

The input data include series of the vertical TEC $I_A(t)$, $I_B(t)$, $I_C(t)$, as well as corresponding series of values of the elevation $\theta_s(t)$ and the azimuth $\alpha_s(t)$ of the LOS. Series of $\theta_s(t)$ and $\alpha_s(t)$ are used to determine the location of the subionospheric point, as well as to calculate the elevation θ of the wave vector \mathbf{K} of the disturbance from the known azimuth α (see formula (5)).

Since the distance between GPS-array elements (from several tens to a few hundred of kilometers) is much smaller than that to the GPS satellite (over 20000 km), the array

geometry at the height near the main maximum of the F_2 -layer is identical to that on the ground.

Linear transformations of the differences of the values of the filtered TEC ($I_B - I_A$) and ($I_B - I_C$) at the receiving points A, B and C are used to calculate the components of the TEC gradient I'_x and I'_y (Afraimovich et al., 1998). The time derivative of TEC I'_t is determined by differentiating $I_B(t)$ at the point B.

The resulting series are used to calculate instantaneous values of the horizontal velocity $V_h(t)$ and the azimuth $\alpha(t)$ of TID propagation. Next, the series $V_h(t)$ and $\alpha(t)$ are put to a statistical treatment. This involves constructing distributions of the horizontal velocity $P(V_h)$ and direction $P(\alpha)$ which are analyzed to test the hypothesis of the existence of the preferred propagation direction. If such a direction does exist, then the corresponding distributions are used to calculate the mean value of the horizontal velocity $\langle V_h \rangle$, as well as the mean value of the azimuth $\langle \alpha \rangle$ of TID propagation.

The correspondence of space-time TEC characteristics, obtained through transionospheric soundings, with local characteristics of disturbances in the ionosphere was considered in detail in a wide variety of publications (Afraimovich et al., 1992; Mercier and Jacobson, 1997) and is not analyzed at length in this study. The most important conclusion of the cited references is the fact that, as for the extensively exploited model of a ‘plane phase screen’, disturbances $dI(x, y, t)$ of TEC faithfully copy the horizontal part of the corresponding disturbance $dN(x, y, z, t)$ of local concentration, independently of the angular position of the source, and can be used in experiments on measuring the wave velocity of TEC.

However, the TEC response amplitude experiences a strong ‘aspect’ dependence caused by the integral character of a transionospheric sounding. As a first approximation, the transionospheric sounding method is responsive only to TIDs with the wave vector \mathbf{K} perpendicular to the direction \mathbf{r} of the LOS. A corresponding condition for elevation θ and azimuth α of \mathbf{K} has the form

$$\tan \theta = -\cos(\alpha_s - \alpha) / \tan \theta_s \quad (5)$$

We used formula (5) in determining the elevation θ of \mathbf{K} from the known mean value of azimuth α by Afraimovich et al. (1998).

The phase velocity modulus V can be defined as

$$V = V_h \times \cos(\theta) \quad (6)$$

Hence at least the dynamic (two-dimensional) characteristics of TEC disturbances (TECS in the case under consideration) may well be referred qualitatively to the corresponding characteristics dN/N of local electron density disturbances (IIDs). Reconstructing the quantitative characteristics of local density disturbances, dN/N , in terms of the solution of an inverse problem of transionospheric sounding is a highly difficult, special problem, constituting the subject of our further investigation.

On the basis of using the transformations described in this section, for each of the GPS arrays chosen for the analysis we obtained the average for the selected time interval values of the following TECS parameters: $\langle\alpha\rangle$ and $\langle\theta\rangle$ – the azimuth and elevation of the wave vector \mathbf{K} ; $\langle V_h\rangle$ and $\langle V\rangle$ – the horizontal component and the phase velocity modulus, the azimuth of a normal to the TECS front α_c from the method reported by Mercier (1986).

4.2 The dynamic characteristics of IIDs

For the PRN05 and PRN30 satellites, Fig. 1c and 1f give an example of the filtered TECS for different spaced stations, and for the GPS satellites on October 5, 2001. It is evident from the figure that the selected typical TEC variations such as TECS are identical and shifted by a certain amount of delay, which makes it possible to calculate the velocity and direction of the IID that causes the observed TEC variations. The panels show the values of the IID velocity V and direction α inferred using the above data processing procedures.

Using different sets of GPS arrays for the entire California region we were able to obtain stable mean estimates of the IID velocity modulus V , horizontal projection V_h and direction α in the horizontal plane, as well as the elevation angle θ of the displacement vector \mathbf{K} in the vertical plane.

Fig. 7. present the distributions of the TECS parameters as determined by the SADM-GPS method, for the "trace" A (on the left; 660 arrays), and for the "trace" B (on the right; 280 arrays). **a, d** – modulus V (line 1) and horizontal component V_h (line 2) of the TECS phase velocity; **b, e** – azimuth α ; **c, f** – elevation θ of the TECS wave vector \mathbf{K} . Same parameters as in Fig.7, but for the "trace" C (on the left; 376 arrays) and for the "trace" D (on the right; 280 arrays) are presented on Fig 8

According to our data, the following values were obtained (using SADM-GPS method): $\langle V_h \rangle = 179$ m/s, $V = 160$ m/s, $\alpha = 360^\circ$, and $\langle \theta \rangle = 22^\circ$ for the trace" A (Fig.7, on the left); $\langle V_h \rangle = 190$ m/s, $V = 165$ m/s, $\alpha = 5^\circ$, and $\langle \theta \rangle = 27.6^\circ$ for the trace" B (Fig.7, on the right); $\langle V_h \rangle = 171$ m/s, $V = 151$ m/s, $\alpha = 5^\circ$, and $\langle \theta \rangle = 24^\circ$ for the trace" C (Fig.8, on the left); and $\langle V_h \rangle = 90$ m/s, $V = 74$ m/s, $\alpha = 360^\circ$, and $\langle \theta \rangle = 20^\circ$ for the trace" D (Fig.8, on the right).

An analysis of the distribution of the azimuths $P(\alpha)$ (Figs. 7b, 7e, 8b, and 8e) shows a clearly pronounced northward direction of TECS displacement. The elevation of the TECS wave vector, determined from the aspect condition (5), has mostly a small positive value (Figs. 7c, 7f, 8c, and 8f).

4.3 The anisotropy and sizes of IIDs

Let us consider in greater detail the "traces" A, B, C, and D. Fig. 6 (a - d) plots the dependencies of the values of the GPS station latitudes N_i on the time $t_{min,i}$, corresponding to each of the TECS detected that day at all GPS stations of the California region used in the analysis (220-260°E; 28-42°N); fig. 6 (e - h) - same as above, but for the station longitudes E_i and $t_{min,i}$. TECS only for a single selected satellite number are considered for each trace.

Figs.6 (a - d) suggest the conclusion that at each given time there are only a few TECS with close values of the coordinates N_i , and there is a clearly pronounced gradual displacement of the subionospheric point in the northward meridional direction. With a knowledge of the range of TECS displacement in latitude and the time interval corresponding to this displacement, it is easy to determine that the meridional projection of the displacement velocity V_N is close to 200 m/s, which is in agreement with estimates obtained using the SADM-GPS method.

On the other hand, the dependencies of the longitude E_i of the TECS observed on $t_{min,i}$ suggest a spatial extent of the traveling irregularity in longitude.

Thus the shape of the observed irregularities ("traces" A, B, C, and D) show up as ellipsoids traveling northward with a velocity of about 200 m/s.

The IID anisotropy was analyzed by determining the "contrast" C (Mercier, 1986). We calculated the ratio $C_{N,E}$:

$$\begin{aligned}
C_{N,E} &= \sigma_N/\sigma_E, \quad \text{if } \sigma_N > \sigma_E \\
C_{N,E} &= \sigma_E/\sigma_N, \quad \text{if } \sigma_E > \sigma_N
\end{aligned}
\tag{7}$$

where σ_N and σ_E are the standard deviations of the corresponding series of the TECS coordinates N_i and E_i . These series were obtained by transforming the initial series N'_i and E'_i by rotating the original coordinate system (N, E) by an angle β :

$$\begin{aligned}
N &= N' \sin \beta + E' \cos \beta \\
E &= -N' \cos \beta + E' \sin \beta
\end{aligned}
\tag{8}$$

Mercier (1986) showed that it is possible to find such a value of the rotation angle β_0 , at which the ratio $C_{N,E}$ will be a maximum and equal to the value of contrast C . This parameter characterizes the degree of anisotropy of the phase interference pattern. The angle β_0 in this case indicates the direction of elongation, and the angle $\alpha_c = \beta_0 + \pi/2$ indicates the direction of the wave vector \mathbf{K} coincident (module 180°) with the propagation direction of the phase front.

Fig. 9 (a, c, e, g) plots the dependencies of the standard deviation $\sigma_N(\alpha)$ of the values of the coordinates of subionospheric points in a topocentric coordinate system, and of the corresponding to t_{min} , on the rotation angle $\alpha_c = \beta_0 + \pi/2$ (β stands for the rotation angle of the original coordinate system) for the "traces" A, B, C, and D (Figs. 5 and 6); Fig. 9 (b, d, f, h) plots the dependencies of the value of the ratio $C_{N,E}$ on $\alpha_c = \beta_0 + \pi/2$. The values of the contrast C are shown by the horizontal dashed line.

It is apparent from the figure that the value of C fluctuates from 6 to 10, and the greatest contrast for the traces under consideration corresponds to the "trace" C and, hence, this trace has the greatest anisotropy.

Furthermore, the direction of elongation of the major axis of the IID ellipse $\beta_0 = -85^\circ$. For the other "traces" the values of the parameter β_0 lie in the range from -80° to -85° . The panels show the mean values of the angles α_c obtained by the method reported in Mercier (1986), and the mean values of α inferred by the SADM-GPS method (Afraimovich, 1997; Afraimovich et al., 1998; 1999; 2000c) for each of the "traces". As is evident from the figure, the values of the angle α , calculated by the two methods, agree to within 5-10°.

We now estimate the horizontal sizes of the IID. With the mean duration of 10 min and the travel velocity of 180 m/s, we obtain the transverse size of the irregularity equal to 108 km. With the value of the contrast $C=9$, the longitudinal size equal to

864 km.

4.4 Estimating the relative IID amplitude

Let us now obtain the mean estimate of the relative amplitude of a local electron density disturbance typified by the IID of October 5, 2001.

A mean TECS absolute amplitude over California equal 0.1 TECU (see Fig.1c, f). As the background value of I_0 , we used the absolute "vertical" TEC value of $I_0(t)$ obtained from IONEX-maps of the TEC (see Fig.10c). These maps with two-hour temporal resolution were constructed using the well-known methods and are placed on the Internet site <ftp://cddisa.gsfc.naa.gov/>.

Fig.10c shows the variations of the absolute "vertical" TEC value $I_0(t)$ for the site with the coordinates 240°E ; 35°N . At the lower time scale in Fig.10, the local time LT is represented for the longitude of 240°E . For comparison Fig.10d present the distribution $N(t)$ of the number of TECS that were detected that day at all GPS stations used in the analysis, with the rms above $\epsilon=0.1 \text{ TECU}$ (this is copy of Fig.5f).

Comparison of Fig. 10c and d reveals that the greatest TECS occurrence probability corresponds to the night-time hours for which the "vertical" TEC value $I_0(t)$ does not exceed 10 TECU .

Hence the relative amplitude of TECS dI/I_0 makes up 1%, that is quite significant for this disturbance period ($\Delta T = 10 \text{ min}$) and exceeds one order of magnitude the amplitude of typical background TEC fluctuations (Afraimovich et al., 2001a).

It is further assumed that the characteristic vertical size of the IID is of the same order as the transverse horizontal size (of about 100 km - see Section 4.3). The vertical extent of the part of the ionosphere that makes the main contribution to the TEC modulation is no less than 500-1000 km. Hence it follows that the relative amplitude dN/N of the local electron density disturbance for IID reaches a considerably large value, 5–10%.

5 Discussion

What is the nature of the ionospheric irregularities that are responsible for the occurrence of TECS, and Do they differ from the known published ionospheric disturbances? We shall try to unravel this situation using the sample statistic obtained in Section 3

and the October 5, 2001 event as an example, because for this event it was possible not only to record a large number of TECS but also to obtain estimates of the size, anisotropy and velocity of isolated ionospheric irregularities that are responsible for the occurrence of TECS (Section 4).

It is significant that, according to Internet data for the concerned region of the USA and for the time interval of October 5, 2001 of our interest, there were not observable meteorological phenomena (site <http://www.solar.ifa.hawaii.edu/Tropical/>), powerful explosions and rocket launchings able to cause TEC variations of the TECS type. The *Titan* – 4 rocket was launched from the "Vandenberg" spaceport (239.5°E; 34.8°N) on October 5 at 21:21 UT (the launching time is shown by the filled triangle in Fig.5f). However, most TECS on that day were observed before the launching time.

As far as seismic activity is concerned, we analyzed the data covering not only the time interval of our interest but also for the period from October 4 to 20, 2001 (<http://wwwneic.cr.usgs.gov/neis/FM/previous/0107.html>). No earthquakes with the magnitude larger than 3.5 were recorded in the region of our interest for the above time interval.

For the October 5, 2001, time interval of our interest, TEC fluctuations similar to TECS detected over California were absent elsewhere on the globe. No solar flare-induced background fluctuations of the TEC disturbance were also revealed. A similar, quiet, behavior over this time interval was also characteristic for the energetic particle flux. We do not present here the relevant data for reasons of space. They may be found on the site <http://www.sel.noaa.gov/ftpmenu/lists.html>.

The geomagnetic situation on October 5, 2001 can be characterized as a weakly disturbed one, which must lead to some increase of the level of TEC background fluctuations; however, this cannot cause any large-scale changes in electron density which are characteristic for the geomagnetically disturbed ionosphere. In the analysis of the geomagnetic situation we used the data from magnetic observatory Victoria (48.52°N; 236.58°E) which, for the time interval 15:00 - 18:00 UT of our interest, recorded a geomagnetic disturbance implying a decrease of the horizontal component of the magnetic field by 100 nT (Fig. 5b).

This disturbance was also accompanied by an increase of the *H*-component fluctuation amplitude in the range of 2-20-min periods (Fig.5c). The variation range of the geomagnetic *Dst*-index for the selected time interval was also relatively small (no

more than 20 nT); however, the period from 08:00 to 15:00 UT showed a clearly pronounced increase in variations of the *Dst*-index that coincided with the period when the *H*-component of the magnetic field was increasing (Fig. 5a).

Hence, the data from magnetic-variation stations do not suggest the conclusion that the observed TECSs are associated with magnetic field variations.

5.1 The difference of TECS from the TEC response to shock-acoustic waves generated due to rocket launchings and earthquakes

First of all, it is important to remark that TECS variations are close in amplitude, form and duration to the TEC response to shock-acoustic waves (SAW) generated during rocket launchings (Calais and Minster, 1996; Calais et al., 1998b; Li et al., 1994; Afraimovich et al., 2000a; 2001b), earthquakes (Calais and Minster, 1995; Afraimovich et al., 2001c), and explosions (Fitzgerald, 1997; Calais et al., 1998a). In this connection, TECS can mask TEC responses to technogenic effects and lead to spurious signals recorded in detection systems for such effects, based on analyzing signals from the global GPS network.

Afraimovich et al. (2000a; 2001b; 2001c) found that spite of a difference of rockets and earthquakes characteristics, the ionospheric TEC response for all such events had the character of an *N*-wave corresponding to the form of a shock wave. The SAW period ΔT is 270–360 s, and the amplitude exceeds the standard deviation of total electron content background fluctuations in this range of periods under quiet and moderate geomagnetic conditions by factors of 2 to 5 as a minimum. The angle of elevation θ of the SAW wave vector varies from 30° to 60°, and the SAW phase velocity V (900–1200 m/s) approaches the sound velocity at heights of the ionospheric *F*-region maximum.

A spatial and temporal processing of data from GPS arrays can be used in selecting these phenomena in order to estimate the propagation velocity of TEC disturbances. In particular, the velocity of IIDs (150–200 m/s) is far less than the SAW velocity (900–1200 m/s) and is most likely to correspond to the propagation velocity of medium-scale background AGW (Kalikhman, 1980; Afraimovich et al., 1998; 1999; Mercier, 1986; Mercier and Jacobson, 1997; Hocke and Schlegel, 1996; Oliver et al., 1997). The SAW and IID phenomena can be distinguished using this attribute, as well as from the

difference of angular characteristics of the disturbance wave vector (see Section 4).

5.2 Can TECS be caused by the E_s -layer ionospheric irregularities that are responsible for S- and QP-scintillations?

As has been pointed out in the Introduction, a large number of publications (e.g., Karasawa, 1985; Titheridge, 1971; etc.), were devoted to the study the "spikes-type" (S-) scintillations.

Bowman (1989) observed quasi-periodic (QP) oscillations of the signal from an orbiting satellite at 150 MHz frequency. The anticipated cause of the occurrence of such QP oscillations is Fresnel diffraction from ionospheric irregularities. Evidently, irregularities giving rise to QP oscillations reside in the E_s level containing a host of small regions (less than 200 m in size) with high electron density separated from one another by a distance of several tens of kilometers. The occurrence of QP oscillations is peaked in the night-time hours. The calculated velocities of irregularities and E_s structures range from 50 to 100 m/s.

The cited authors point out that transionospheric signal variations of this kind are observed mostly at night and are most likely caused by the irregularities located in the E_s -layer. This brings up the question of whether the TECS recorded by us are able to be caused by such ionospheric irregularities. At this point it should be noted that TECS are also observed mostly at night, and their velocities (on the order of 100 km/s) are close to those obtained by Karasawa (1985), Titheridge (1971), and Bowman (1989).

In order to verify the validity of this TECS model for the October 5, 2001 event we availed ourselves of the data (placed on the site <http://spidr.ngdc.noaa.gov/spidr/>) from the ionospheric station Point Arguello located in the center of the region of our interest.

Fig.10a present the values of the critical frequencies f_0F_2 – heavy dots; f_0E_s – crosses; f_0E –shaded triangles, measured on October, 5, 2001 at ionospheric station Point Arguello ($239.4^\circ E$; $34.6^\circ N$); Fig.10b – variations of virtual height $h'E$ – shaded triangles, $h'E_s$ – crosses.

An analysis of the dependence of critical frequencies and effective heights of reflections from the F - and E_s -regions showed that during 08-14 UT when the largest number of TECS was recorded, reflections from the E_s -layer were absent altogether

(cf. panels **a**, **b**, **d**).

Thus we did not obtain any direct confirmation of the fact that TECS were caused by intense ionospheric irregularities located in the E_s -layer. The question of the origin of the IID that are responsible for TECS remains open.

It should be noted that direct comparison of our results with the data obtained by Karasawa (1985), Titheridge (1971), and Bowman (1989), is made difficult by the fact that the overwhelming amount of earlier data was obtained for amplitude, rather than phase, scintillations. On the other hand, extracting data on amplitude variations of GPS signals from Internet RINEX-files is highly difficult (Gurtner, 1993).

To understand the nature of TECS requires invoking data from different, independent diagnostic tools, including incoherent scatter radars, ionosondes, magnetometers, etc.

6 Conclusion

Main results of this study may be summarized as follows:

1. TECS constitute a rare event that occurs mainly in the night-time in the spring and autumn periods, in a weakly disturbed or quiet geomagnetic situation.
2. In the time region, TECS represent single negative aperiodic abrupt changes of TEC with a duration of about 10-20 min; the mean value of the TECS amplitude exceeds the mean value of the TEC variation amplitude by a factor of 4-5 as a minimum and is 0.2 TECU .
3. TECS represent a local phenomenon with a typical radius of spatial correlation not larger than 500 km.
4. The TECS we recorded on October 5, 2001, were caused by isolated ionospheric irregularities of the ellipsoid shape, with the direction of elongation of the major axis of the ellipse on the order of -85° . IIDs travel in a direction perpendicular to their elongation (northward in the case under consideration) with the mean velocity $\langle V \rangle = 160 \text{ m/s}$, which corresponds to the velocity of medium-scale AGW (of about 100-200 m/s). The size of the observed irregularities is 100 km by 800 km, respectively.

We are aware that this study has revealed only the key averaged patterns of this phenomena, and we hope that it would give impetus to a wide variety of more detailed investigations.

ACKNOWLEDGMENTS

We are indebted to Dr. N.T. Afanasyev for participating in discussions. We thank O.S. Lesyuta and S.V. Voeykov for help in organizing the experiment. We are also grateful to V.G. Mikhalkovsky for his assistance in preparing the English version of the manuscript. This work was done with support under RFBR grant of leading scientific schools of the Russian Federation No. 00-15-98509 as well as Russian Foundation for Basic Research grants No. 00-05-72026 and 02-05-64570.

References

- [1] Afraimovich, E. L., Terechov A. I., Udodov M. Yu. and Fridman S. V., Refraction distortions of transionospheric radio signals caused by changes in a regular ionosphere and by travelling ionospheric disturbances, *J. Atmos. and Terr. Phys.*, 54, 1013–1020, 1992.
- [2] Afraimovich, E. L. Statistical angle-of-arrival and doppler method (SADM) for determining characteristics of the dynamics of the transionospheric radio signal interference pattern, *Acta Geod. Geoph. Hung.*, 32, N 3-4, 461–468, 1997.
- [3] Afraimovich, E. L., K. S. Palamartchouk, and N. P. Perevalova, GPS radio interferometry of travelling ionospheric disturbances. *J. Atmos. and Sol.- Terr. Phys.*, 60, N12, 1205–1223, 1998.
- [4] Afraimovich, E. L., Boitman O. N., Zhovty E. I., et al. Dynamics and anisotropy of traveling ionospheric disturbances as deduced from transionospheric sounding data, *Radio Sci.*, 34, N2, 477–487, 1999.
- [5] Afraimovich E.L., E.A.Kosogorov, K.S.Palamarchouk, N.P. Perevalova, and A.V. Plotnikov. The use of GPS arrays in detecting the ionospheric response during rocket launchings. *Earth, Planets, and Space*, 52, N11, 1061–1066, 2000a.
- [6] Afraimovich, E. L., The GPS global detection of the ionospheric response to solar flares. *Radio sci.*, 35, N6, 1417–1424, 2000b.
- [7] Afraimovich E. L., K. S. Palamartchouk, and N. P. Perevalova, Statistical angle-of-arrival and doppler method for GPS interferometry of TIDs, *Adv. Space Res.*, 26, N6, 1001–1004, 2000c.
- [8] Afraimovich E. L., Kosogorov E. A., Lesyuta O. S. et al. Geomagnetic control of the spectrum of traveling ionospheric disturbances based on data from a global GPS network. *Ann. Geophys.*, 19, N 7, 723–731, 2001a.
- [9] Afraimovich, E. L., Kosogorov E. A., Perevalova N. P., and Plotnikov A. V. The use of GPS-arrays in detecting shock-acoustic waves generated during rocket launchings. *J. Atmos. and Sol.-Terr. Phys.*, 63, N18, 1941–1957, 2001b.

- [10] Afraimovich, E. L., Perevalova N. P., Plotnikov A. V. and Uralov A. M, The shock-acoustic waves generated by earthquakes. *Ann. Geophys.*, 19, 395–409, 2001c.
- [11] Bowman G.G., Quasi-periodic scintillations at mid-latitudes and their possible association with ionospheric E-sporadic structures, *Ann. Geophys.*, 7, N 3, 259–268, 1989.
- [12] Calais, E. and Minster, J.B. GPS detection of ionospheric perturbations following the January 1994, Northridge earthquake. *Geophys. Res. Lett.*, 22, 1045–1048, 1995.
- [13] Calais, E., and Minster, J.B. GPS detection of ionospheric perturbations following a Space Shuttle ascent. *Geophys. Res. Lett.*, 23, 1897–1900, 1996.
- [14] Calais, E., Minster, J.B., Hofton, M.A., and Hedlin, M.A.H. Ionospheric signature of surface mine blasts from Global Positioning System measurements. *Geophys. J. International*, 132, 191–202, 1998a.
- [15] Calais, E., Minster, J.B., and Bernard, J. GPS, Earthquake, the ionosphere and Space Shuttle. *Physics of Earth and Planet*, 105, 167–181, 1998b.
- [16] Fitzgerald, T.J. Observations of total electron content perturbations on GPS signals caused by a ground level explosion. *J. Atmos. and Terr. Phys.*, 59, 829–834, 1997.
- [17] Gurtner, W., RINEX: The Receiver Independent Exchange Format Version 2, [urlhttp://igsb.jpl.nasa.gov:80/igsb/data/format/rinex2.txt](http://igsb.jpl.nasa.gov:80/igsb/data/format/rinex2.txt), 1993.
- [18] Hocke, K., and K. Schlegel, A review of atmospheric gravity waves and traveling ionospheric disturbances: 1982-1995, *Ann. Geophys.*, 14, 917–940, 1996.
- [19] Hofmann-Wellenhof, B., H. Lichtenegger, and J. Collins, *Global Positioning System: Theory and Practice*, Springer-Verlag Wien, New York, 1992, 327 p.
- [20] Kalikhman A. D. Medium-scale traveling ionospheric disturbances and thermospheric winds in the F-region. *J. Atmos. Sol. Terr. Phys.*, 42, 697–703, 1980.
- [21] Karasawa Y., Yasukawa K. and Yamada M. Ionospheric scintillation measurements at 1.5 GHz in mid-latitude region, *Radio Sci.*, 20, N3, 643–651, 1985.
- [22] Klobucar J. A., Ionospheric time-delay algorithm for single-frequency GPS users, *IEEE Trans. on Aerospace and Electronic systems*, AFS-22-N3, 325–331, 1986.

- [23] Li, Y.Q., Jacobson, A.R., Carlos, R.C., Massey, R.S., Taranenko, Y.N., and Wu, G. The blast wave of the Shuttle plume at ionospheric heights. *Geophys. Res. Lett.*, 21, 2737–2740, 1994.
- [24] Mannucci, A.J., C.M. Ho, U.J. Lindqwister, T.F. Runge, B.D. Wilson and D.N. Yuan. A global mapping technique for GPS-driven ionospheric TEC measurements. *Radio Sci.*, 33, 565–582, 1998.
- [25] Mercier, C. Observations atmospheric gravity waves by radio interferometry, *J. Atmos. and Terr. Phys.*, 48, 605–624, 1986.
- [26] Mercier, C. and Jacobson, A.R. Observations of atmospheric gravity waves by radio interferometry: are results biased by the observational technique. *Ann. Geophys.*, 15, 430–442, 1997.
- [27] Oliver, W. L., Otsuka Y., Sato M., Takami T., and Fukao, S. A climatology of F region gravity waves propagation over the middle and upper atmosphere radar. *J. Geophys. Res.*, 102, 14449–14512, 1997.
- [28] Titheridge J. E. The diffraction of satellite signals by isolated ionospheric irregularities, *J. Atmos. and Terr. Phys.*, 33, 47–69, 1971.

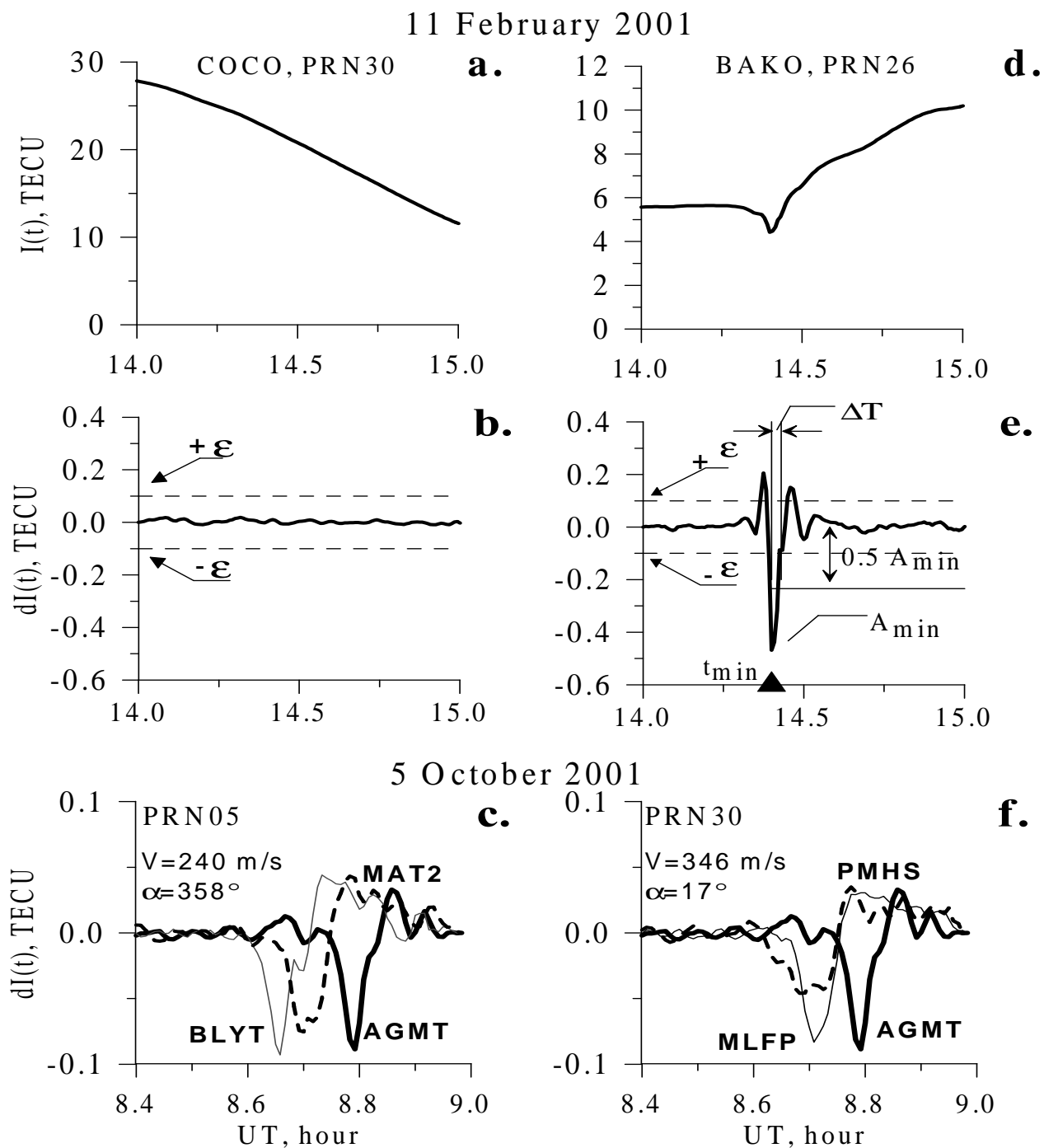


Figure 1: An illustration of the selection of TECS: **a** – typical $I(t)$ series containing no TECS; **b** – filtered $dI(t)$ -series. Panels **d** and **e** – same but for the $I(t)$ -series containing TECS. Shown in panels **a** and **d** are the station names and GPS satellite numbers. Levels of limitation in TECS amplitude ϵ are shown in panels **b** and **e** by horizontal lines. Panel **e** shows the minimum value of the amplitude A_{min} , the time t_{min} corresponding to this amplitude, and the time duration ΔT of TECS. Panels **c** and **f** (for PRN05 and PRN30, respectively) present the filtered TECS for spaced GPS stations.

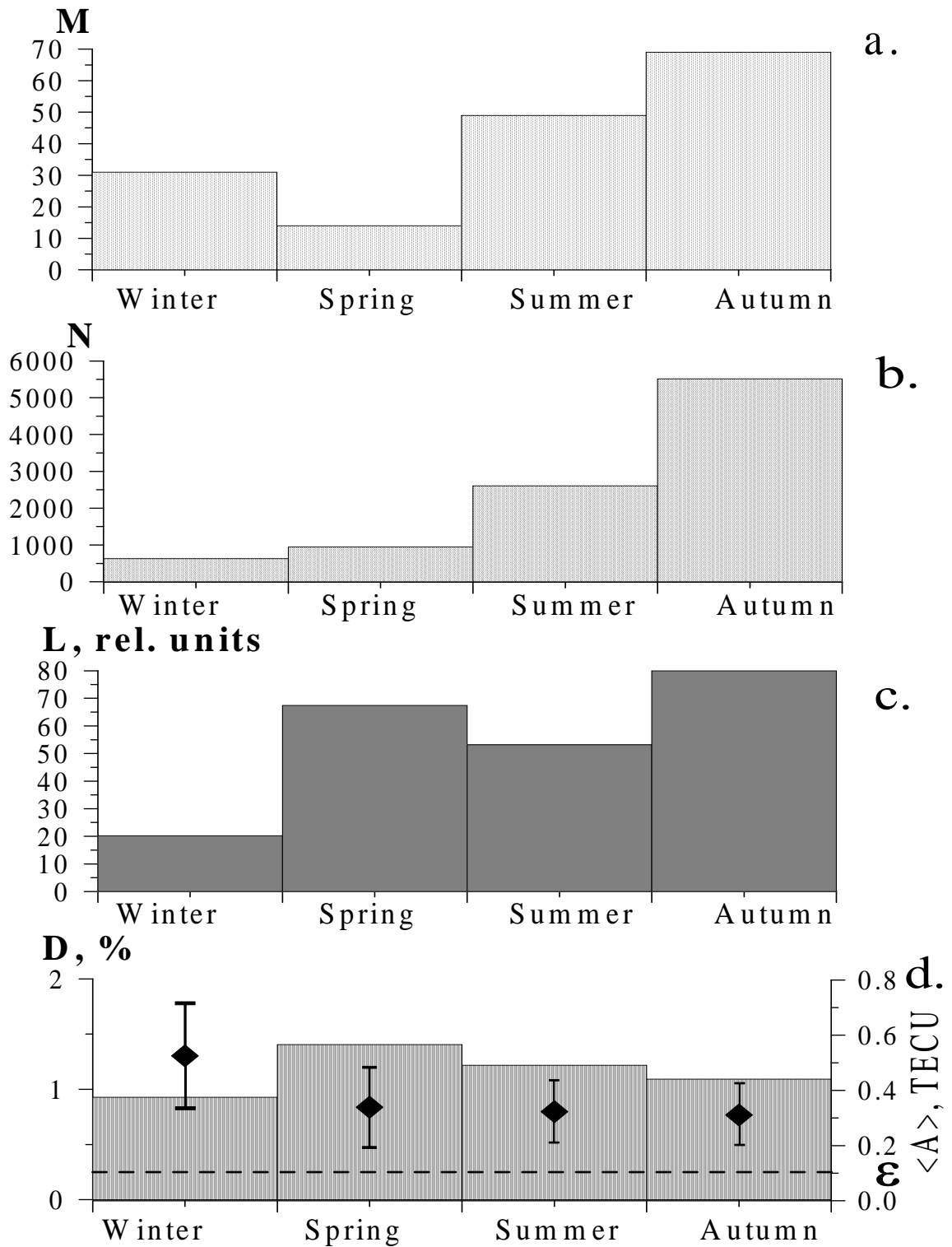


Figure 2: Seasonal dependence of the density and maximum amplitude of TECS: **a** – number of days M of observation versus time of the year; **b** – number of TECS N ; **c** – mean number of TECS per day $L = N/M$. **d** – relative TECS density D obtained as the ratio of the number of TECS N to the number of receiver-satellite LOS. Diamonds in panel **d** show the mean values of $\langle A \rangle$ of the minimum amplitudes A_{min} for each season, and vertical lines show their standard deviations. The dashed horizontal line shows the threshold in amplitude ($\epsilon = 0.1$ TECU).

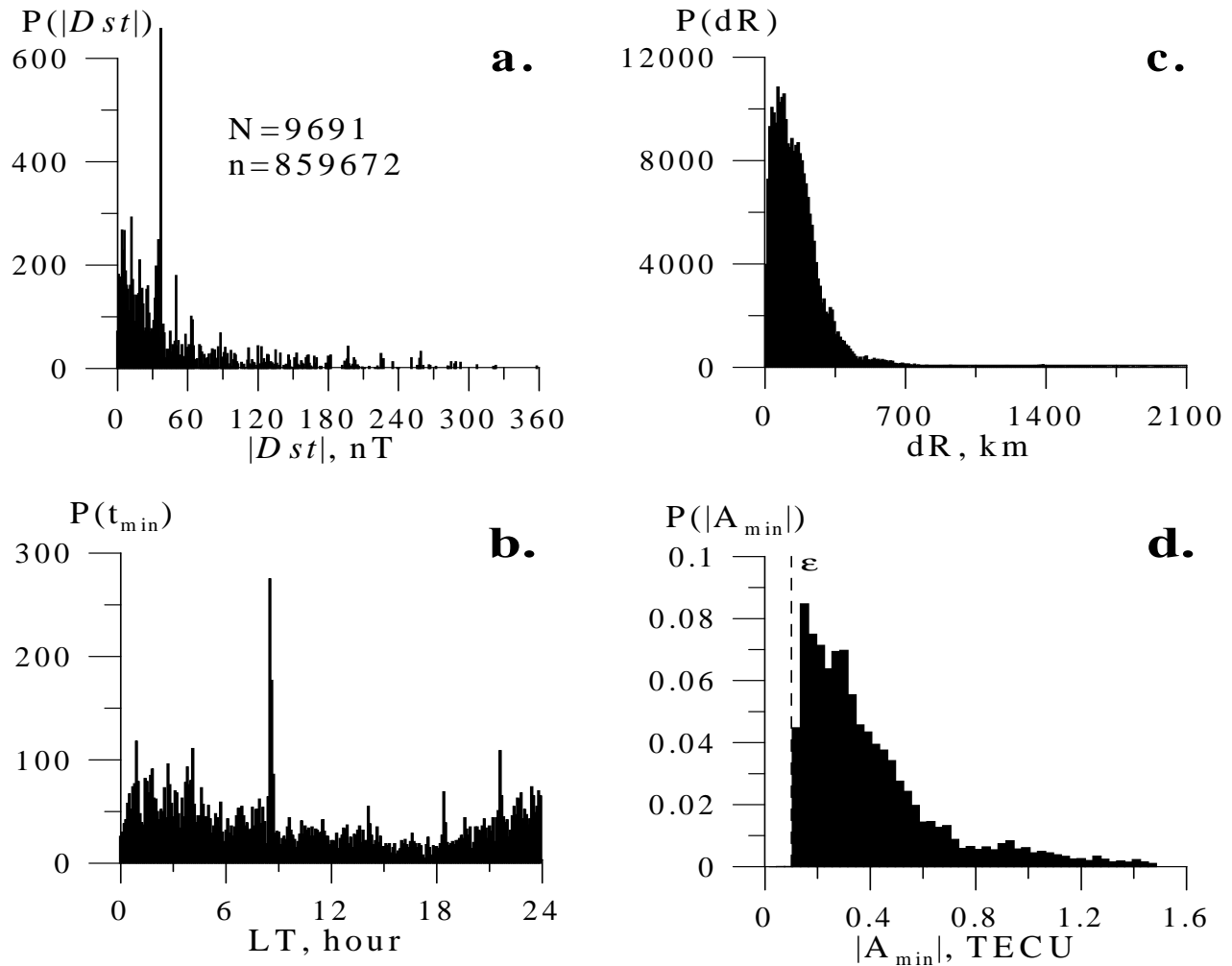


Figure 3: Statistic of TECS: **a** – dependence of the number of TECS on the modulus of the Dst -index; **b** – diurnal distribution $P(t_{min})$ of the times t_{min} corresponding to the minimum amplitude A_{min} of the TECS; **c** – histogram $P(dR)$ of the number of cases where TECS within one 2.3-hour time interval were observed at any two GPS stations, with the distance dR between them; **d** – distribution $P(|A_{min}|)$ of the minimum amplitude A_{min} of TECS. The vertical dashed line in panel **d** shows the threshold in amplitude $\epsilon = 0.1$ TECU. Panel **a** shows the number N of the detected TECS, and the total number n of receiver-satellite LOS.

5 October 2001
08:00 - 10:00 UT

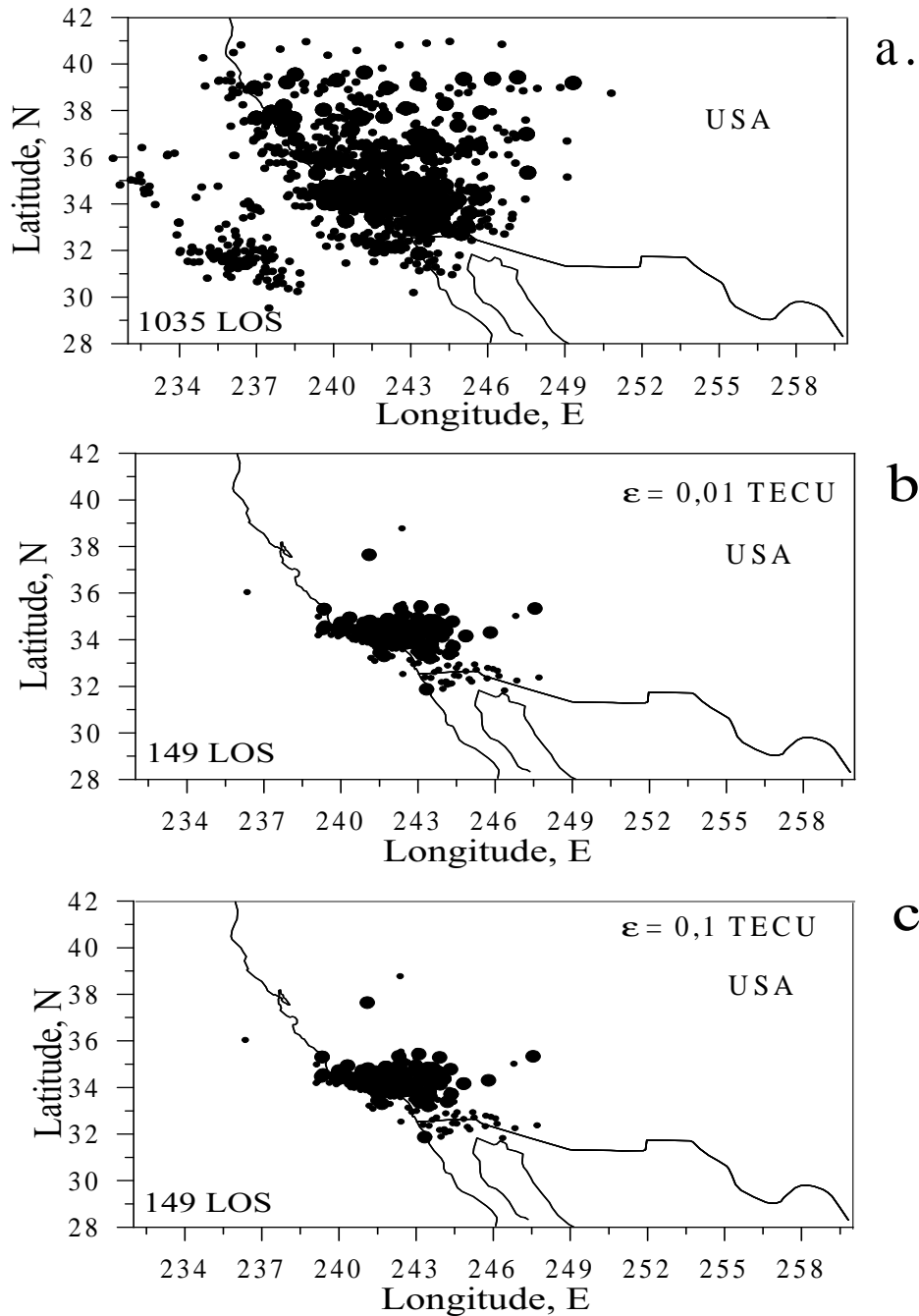


Figure 4: Geometry of the experiment on detection of TECS on October 5, 2001 in California, USA, from 08:00 to 10:00 UT. Heavy dots show the GPS stations, and small dots show the location of subionospheric points for receiver-satellite LOS. Panel a shows the stations and subionospheric points for all LOS's. Panels b and c show the stations and subionospheric points where the TEC variations revealed TECS with an amplitude exceeding the specified threshold $\epsilon = 0.01 \text{ TECU}$ (b), and $\epsilon = 0.1 \text{ TECU}$ (c). Numbers in all panels show the total number of LOS's shown in the panel.

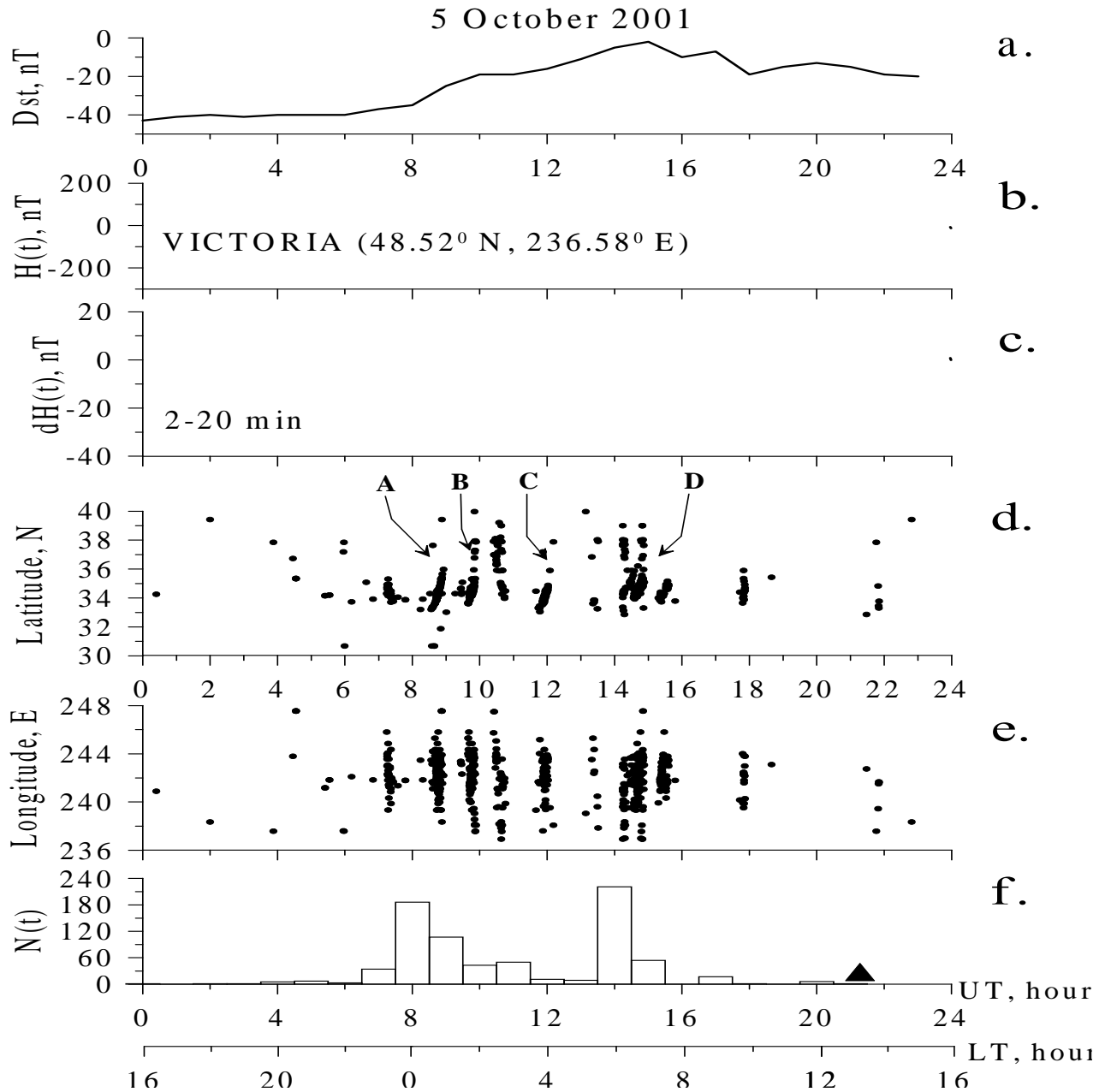


Figure 5: Geomagnetic field D_{st} -variations (a) October 5, 2001. $H(t)$ -variations of the horizontal component of the geomagnetic field as recorded at station Victoria ($236.58^{\circ}E$; $48.52^{\circ}N$) – b. $dH(t)$ -variations of the horizontal component of the geomagnetic field, filtered from the series $H(t)$ in the range of periods of 2–20 min – c. d – the distribution of the values of the GPS station latitudes from time t_{min} , corresponding to each of the TECS detected that day by all GPS stations of the California region that were used in the analysis (220 – $260^{\circ}E$; 28 – $42^{\circ}E$); e — same as in 5d, but for the station longitudes and t_{min} ; f – the distribution $N(t)$ of the number of TECS that were detected that day at all GPS stations used in the analysis, with the rms above $\epsilon=0.1$ TECU. The letters A, B, C, and D in Fig. 5d label the TECS "traces" that are presented in Fig. 6 on a smaller time scale. Shaded triangle in panel f signs the *Titan*–4 launch time 21:21 UT from Vanderberg cosmodrome ($239.5^{\circ}E$; $34.8^{\circ}N$).

5 October 2001

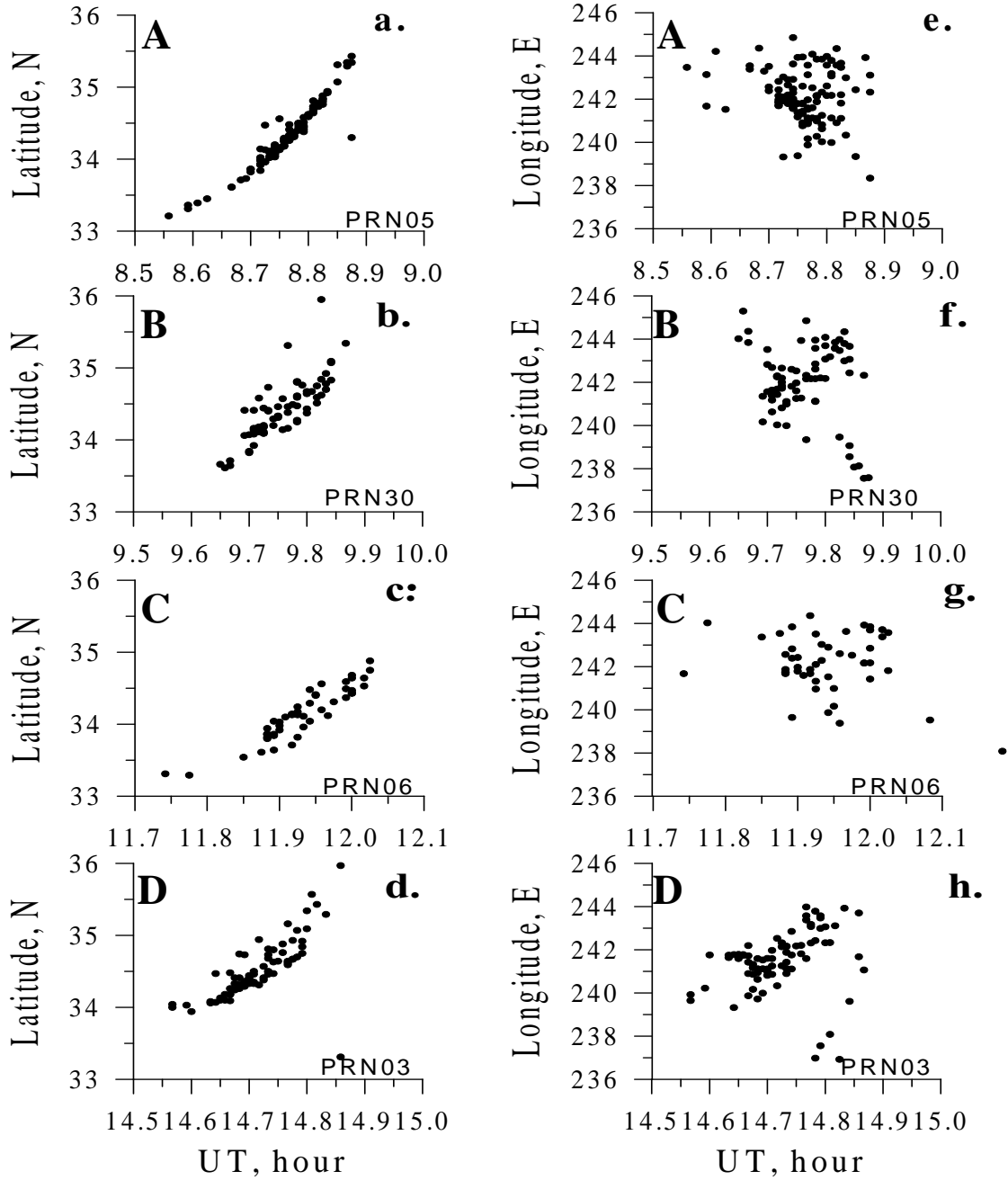


Figure 6: a, c, e, g – The distribution of the values of the GPS station latitudes from time t_{min} , corresponding to each of the TECS detected that day; the letters A, B, C and D label the TECS "traces" that are presented in Fig.5 on a longer time scale; b,d, f, h - same as in Fig.6 (a, c, e, g), but for the station longitudes and t_{min} .

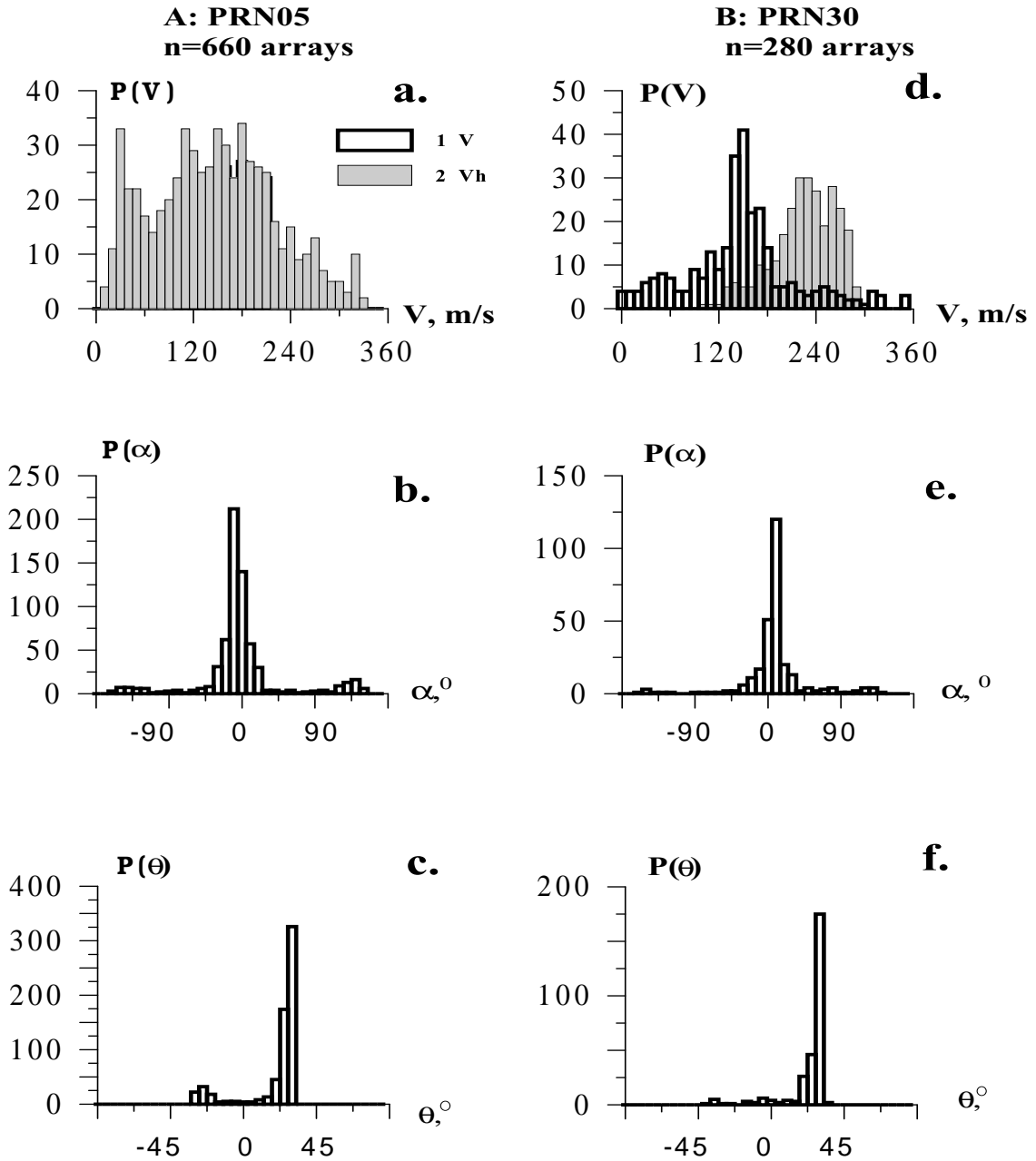


Figure 7: Distributions of the TECS parameters as determined by the SADM-GPS method, for the "trace" A (on the left; 660 arrays), and for the "trace" B (on the right; 280 arrays). **a, d** – modulus (line 1) and horizontal component (line 2) of the TECS phase velocity; **b, e** – azimuth α ; **c, f** – elevation θ of the TECS wave vector \mathbf{K} .

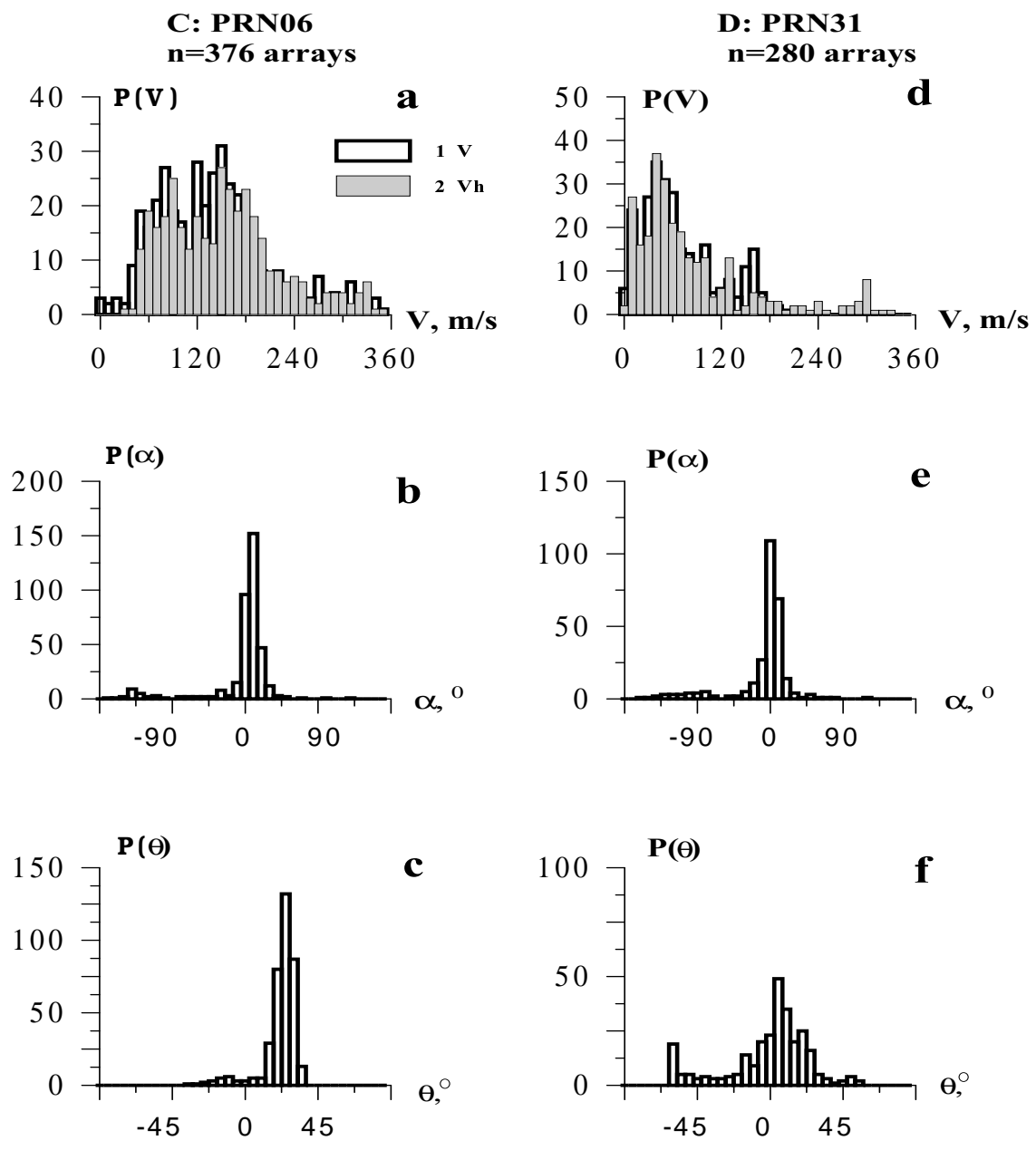


Figure 8: Same as in Fig.7, but for the "trace" C (on the left; 376 arrays), and for the "trace" D (on the right; 280 arrays).

5 October 2001

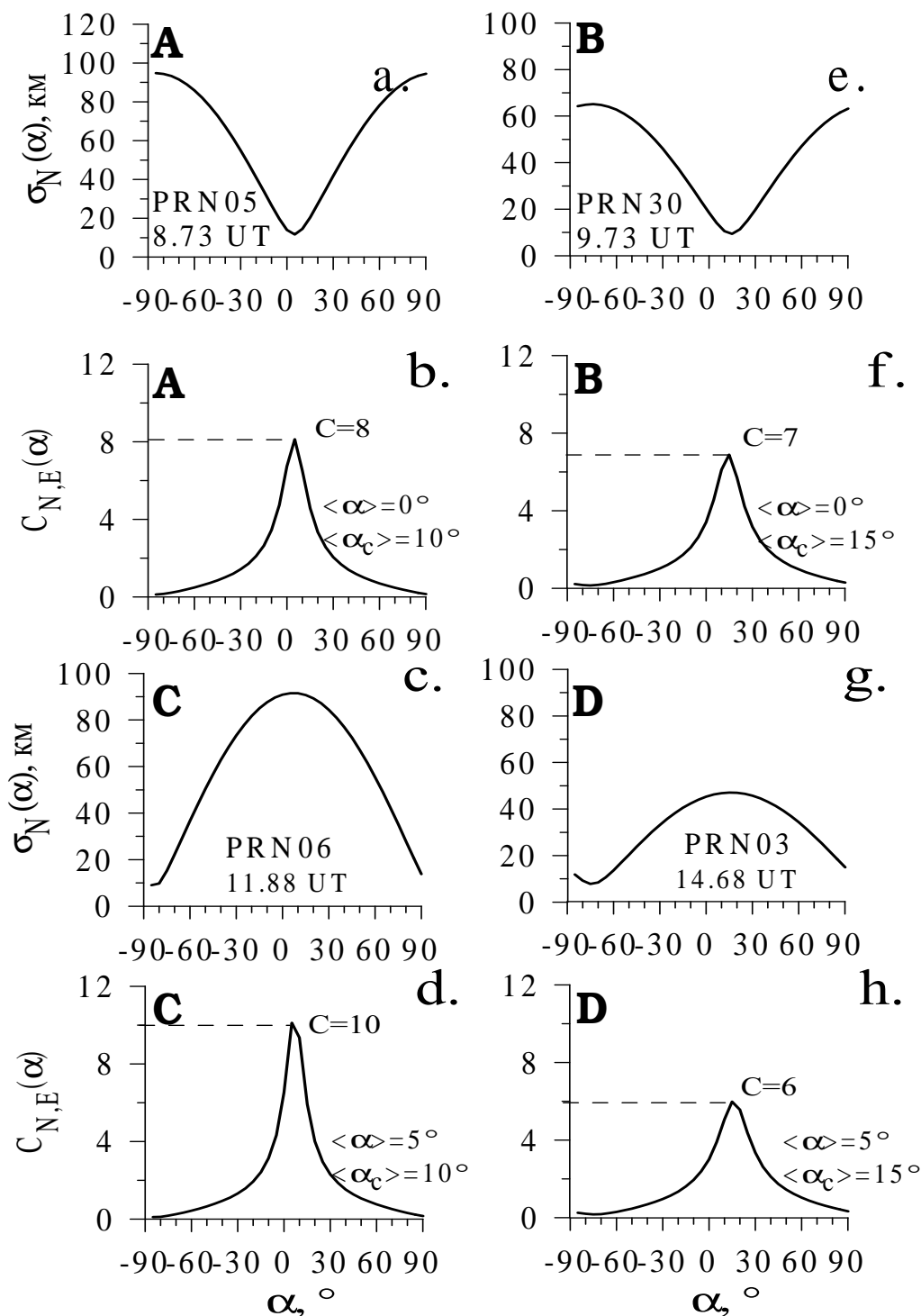


Figure 9: a, c, e, g – the dependencies of the standard deviation $\sigma_N(\alpha)$ of the values of the coordinates of subionospheric points in a topocentric coordinate system, and of the corresponding to t_{min} , on the rotation angle $\alpha_c = \beta_0 + \pi/2$ (β stands for the rotation angle of the original coordinate system) for the "traces" A, B, C, and D (Fig. 6); b, d, f, h – the dependencies of the value of the ratio $C_{N,E}$ on $\alpha_c = \beta_0 + \pi/2$. The values of the contrast C are shown by the horizontal dashed line.

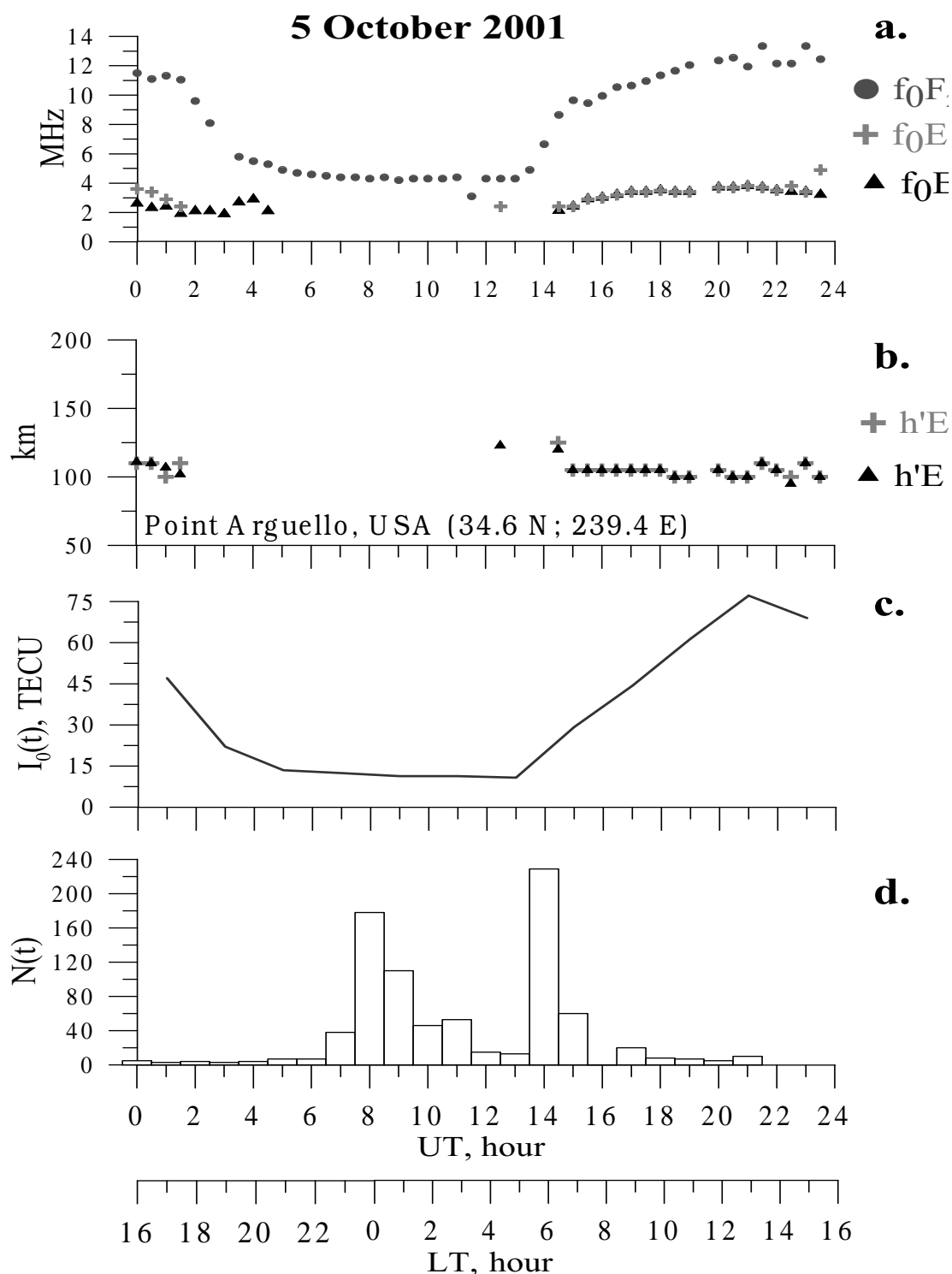


Figure 10: **a** – values of the critical frequencies f_0F_2 – heavy dots; f_0E_s – crosses; f_0E –shaded triangles, measured on 5 October, 2001 at ionospheric station Point Arguello ($239.4^\circ E$; $34.6^\circ N$); **b** – variations of virtual heights $h'E$ – shaded triangles, $h'E_s$ – crosses. **c** – variations of the absolute "vertical" TEC value $I_0(t)$ for the site with the coordinates $240^\circ E$; $35^\circ N$, obtained from IONEX-maps of TEC; **d** – the same as Fig.5f.